

Interplay between elastic interactions in a core-shell model for spin-crossover nanoparticlesH. Oubouchou,^{1,2} A. Slimani,¹ and K. Boukheddaden^{1,*}¹*Groupe d'Etudes de la Matière Condensée UMR8635, CNRS-Université de Versailles /St. Quentin en Yvelines, 45 Avenue des Etats Unis, F78035 Versailles Cedex, France*²*Centre de Recherche Scientifique et Technique en Soudage et Contrôle, Division des Procédés Electriques et Magnétiques, Route de Dély-Ibrahim - BP 64 Chéraga, Alger, Algeria*

(Received 2 March 2012; revised manuscript received 26 January 2013; published 7 March 2013)

A coupled spin deformation model for spin-crossover (SC) materials, consisting of distortable 2D square-shaped lattices, whose sites may be occupied by high-spin (HS) or low-spin (LS) atoms, is studied by Monte Carlo simulations. To be consistent with the experimental studies, we have studied shell-free and core-shell nanoparticles. In the case of shell-free nanoparticles, we constrained the surface of the nanoparticle (one layer) to be in the HS state from the electronic and the elastic point of view because the surface atoms have weaker ligand-field energy than those of the bulk. We then investigated the size effects and found that the thermal hysteresis width ΔT and the transition temperature T_{eq} follow the respective universal laws, $\Delta T \propto \sqrt{(L - L_0)}$ and $T_{\text{eq}} \propto \sqrt{\ln(L - L_c)}$, where L is the nanoparticle size. These laws hold independently of the sweeping rate of temperature. In a second stage, we studied the effect of a soft shell on the thermal properties of the core shell nanoparticle for which we have investigated the thermodynamic properties at various sizes of the shell. We find that the thermal hysteresis shifts downwards and the corresponding width increases; a result that contrasts with that of shell-free nanoparticles. In addition, we have observed that large shell size hinders the domain formation upon the first-order transition, although the transition is still of first order. These behaviors originate from the elastic stress produced by the shell on the bulk of the nanoparticle, and are identified through the spatial distribution of the internal stress upon the thermal transition. Moreover, we studied the effect of the shell size on the relaxation of the photoinduced metastable HS fraction at low temperature. At this end, a preliminary optimization of the structure of the nanoparticle is performed. We then evidenced that increasing the size of the shell results in an acceleration of the relaxation process. This behavior is in excellent agreement with recent data reported on core shell nanoparticles of Prussian Blue analogs.

DOI: [10.1103/PhysRevB.87.104104](https://doi.org/10.1103/PhysRevB.87.104104)

PACS number(s): 78.67.Rb, 75.30.Wx, 75.75.Fk, 65.80.-g

I. INTRODUCTION

The thermally induced spin crossover (SC) transition between the low-spin (LS) and the high-spin (HS) states of Fe(II) complexes with suitable ligands are examples of molecular bistable solids. They have been studied¹⁻⁹ for many years due to their promising applications as materials for information storage. Their bistability, originating from intramolecular vibronic coupling, can be enhanced by intermolecular interactions. At the solid state, the elastic interactions constitute the basic mechanism from which the richness of the behavior of these systems is originated. They lead to rather abrupt thermal spin transitions and, in many cases, even to hysteresis behavior denoting a first-order phase transition or a two-step spin transition,¹⁰⁻¹² instead of a gradual transition corresponding to the simple Boltzmann distribution between two states, which is generally obtained in highly diluted crystals (i.e., noncooperative systems).

In recent years, there has been growing interest in the field of SC solids. Under various constraints, such as temperature² or pressure^{13,14} variations, irradiation by visible light^{15,16} or magnetic field,¹⁷ SC solids can be switched from LS to HS state, and conversely.^{1,5} For example, Fe^{II} SC compounds¹⁸ are diamagnetic ($S = 0, \text{LS}$) and paramagnetic ($S = 2, \text{HS}$) in the low- and high-temperature phases, respectively. The SC transition involves both electronic transformation (spin and orbital) and structural modifications. In the case of these Fe^{II} compounds, the metal-ligand bond lengths change by about 0.2 Å ($\approx 10\%$) and the ligand-metal-ligand bond angles by

$0.5^\circ - 80^\circ$.^{19,20} Optical properties are also changed^{15,21,22} with usually a colorless HS and a strongly colored LS state in the case of Fe^{II} systems. Consequently, magnetic and optical measurements^{23,24} are the major experimental techniques used for quantitative investigations of the spin transitions. In many cases, elastic interactions between the SC units are strong enough to induce hysteresis at the thermal spin transition,⁶ which occurs as a first-order phase transition. Such “switchable” molecular solids are promising in terms of optical data storage.⁸

Since a few years, the synthesis and the design of SC nanoparticles have become possible and several interesting behaviors have been reported.^{25,26} The experimental results, for most of these studies, confirmed the expected narrowing of hysteresis loop and in some cases, the collapse of the loop below some “critical size,” but very few of them provided a coherent set of data over the relevant size range, that is, above and below the critical size. In addition, the samples usually present a rather wide distribution of sizes, various shapes, and particles were often aggregated in various manners. All these features obviously impact the switching behavior of the SC nanoparticles and made the investigation on the properties of a unique nanoparticle a very challenging goal. From the theoretical point of view, there were a few studies of the thermal and photo-switching properties of SC nanoparticles^{27,28} that aimed at reproducing the collapse of the hysteresis effects at the critical size of the particles. In addition, although not discussed in the experimental papers, chemical aging effects have been also recently observed in the SC nanoparticles, which render

their study a little bit more complicated from the experimental point of view. Among the theoretical investigations, we have recently published a Monte Carlo (MC) study of a 2D finite size Ising-like model with specific states of the atoms located at the surface.²⁹ There, we found that the model well reproduces the experimental behavior of the transition temperature and the hysteresis loops of nanoparticles of $\text{Fe}(\text{pyrazine})\{\text{Pt}(\text{CN})_4\}$.³⁰ However, this model does not account for the elastic properties of the SC nanoparticles. In particular, although the specific HS electronic state of the surface atoms was taken into account, the phonon dispersion at the surface (that is, the specific elastic constant) at the surface must be also different from that of the bulk. In addition, in such Ising-like approaches, an increase of the number of the HS layers at the surface does not impact the thermal dependence of the HS fraction. This means that these models are not adapted for the description of core/shell problems, due to the absence of the elastic interaction between the spin units.

These various aspects of SC nanoparticles have been suggested by recent experimental investigations.³⁰⁻³⁴ General features of SC nanoparticles with well-controlled size show the existence of a hysteresis loop above some critical. In addition to the expected narrowing of the hysteresis loop on decreasing size, most of the systems display a sizable lowering of the transition temperature and an increase of the residual HS fraction. The latter features are explained by the different coordination of the surface atoms, including water molecules instead of the organic ligands. The latter, experiences a weaker ligand-field forcing them to stay in the HS state and, consequently, lower the transition temperature of the particle through a “negative pressure” effect. For practical reasons, the present investigation was performed on 2D networks connected by springs. Not only nearest-neighbor interactions are considered but also next-nearest-neighbors in order to keep the mechanical stability of the lattice. We performed MC simulations using an elastic model combining electronic and deformation degrees of freedom. In this model, each molecule is described by a two-states fictitious spin describing the low-spin and the high-spin states, a view inspired by the Ising-like Hamiltonian (interacting two-level systems), widely used in literature to describe the equilibrium^{35,36} and nonequilibrium³⁷ properties of SC solids.

Recently, however, several experimental studies have addressed the problem of core/shell nanoparticles of SC and Prussian Blue analogs^{38,39} as well as that of SC nanoparticles embedded in various types of matrices. The problem of the influence of the rigidity difference between the infinite matrix and SC nanoparticles has been studied recently using a different elastic model. However, the true case of the core/shell problem, which implies the study of the influence of the shell size on the SC properties of the core (the active part), has never been studied.

From the theoretical point of view, recent investigations using distortable lattices, based on pure elastic Hamiltonians⁴⁰ or on models combining spin-lattice interactions^{28,41,42} have shown that the volume change induced by the spin transition affects considerably the transition and can even change the nature of the phase transition. Since a simulation based on a model of systems interacting via a long-range distant potential is usually very time consuming because the particles

are allowed to move freely, here, we adopt an alternative approach in which the SC solid is modeled as a network of nodes with the fixed topology of a 2D square lattice. Apart from moving the nodes stochastically, the MC algorithm also changes the spin states at the nodes within the framework of a canonical ensemble. The present study is performed by using an anharmonic interatomic potential that we have used recently when we solved exactly a set of coupled bistable oscillators in the frame of the transfer integral method.⁴³

The paper is organized as follows. In Sec. II, we define the model, describe the simulation technique, and explain our choice of interaction parameter values. In Sec III, we consider the core size dependence of the HS fraction arising from nanoparticles with one HS layer as a shell. In Sec. IV, we study the thermodynamic properties of core-shell nanoparticles with variable shell sizes (variable number of shell layers) at fixed core size. For both cases, we give a detailed discussion of the thermodynamic properties of the HS fraction and its relation to the elastic properties of the lattice. Spatial distributions of the HS fraction and that of the elastic strain along the hysteresis width are presented and discussed. Moreover, we calculate the time dependence of the photoinduced HS fraction at low temperature, the relaxation properties of which are discussed in comparison with the data of the shell free nanoparticles. In Sec. V, we conclude.

II. THE MODEL: THEORETICAL BACKGROUND AND CHOICE OF THE PARAMETERS

We consider here a square lattice of SC units (see Fig. 1) in which each of them may have two states, HS and LS, described by an associated fictitious spin S , the values of which are given by $S = +1$ (HS) and -1 (LS). Hence we studied systems of $N = L^2$ nodes, with $L = 6, 10, 18, 40,$ and 60 . Initially, these nodes were put onto the sites of an ideal square lattice with the lattice constant of a pure HS state. Throughout the simulation, we used open boundary conditions in order to take account of surface effects. We will come later to a discussion of this aspect.

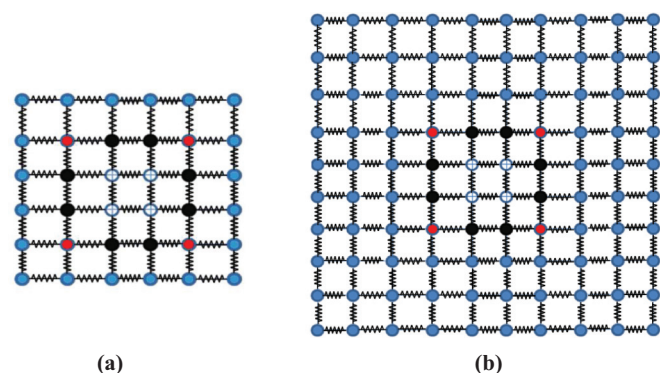


FIG. 1. (Color online) Elastic 2D lattice representing the two types of SC nanoparticles considered in the work: (a) with a shell made of one layer of fixed HS atoms or (b) with a shell made of several HS layers. Red sites are SC atoms having two fixed HS nearest neighbors, black atoms have one fixed HS atom, and white sites have no fixed HS state as a neighbor. The spring linking the next-nearest neighbors have been omitted for clarity reasons.

The total Hamiltonian of the system in the case of Fig. 1(a) accounting for electronic and elastic contributions reads

$$H = \sum_i \frac{1}{2} [\Delta - k_B T \ln(g)] S_i + \sum_{(i,j)} A_{ij} [r_{ij} - R_0(S_i, S_j)]^2 + \sum_{(i,k)} B_{ik} [r_{ik} - R'_0(S_i, S_k)]^2 \text{ and}$$

$$S(i, N) = S(N, j) = S(i, 1) = S(1, j) = +1, \quad (1)$$

where the first term of the Hamiltonian (1) contains the energetic contribution Δ , arising from the difference of ligand-field energy between the two states and the entropic contribution $-k_B T \ln g$ coming from the electrovibrational degeneracy g of the high-spin state. The second and the third terms account for elastic interactions between nearest-(nn) and next-nearest-neighbours (nnn) SC units, respectively. The latter are introduced here to keep the stability of the lattice. The Hamiltonian corresponding to the case of Fig. 1(b) is easily obtained from Eq. (1) by adding the constraint $S(i, N + \alpha) = S(j, N + \alpha) = S(i, 1 + \alpha) = S(1 + \alpha, j) = +1$, with $\alpha = 1, N_S$, where N_S is the number of the HS shell layers.

The nodes of the lattice of Fig. 1 are linked by springs. The equilibrium lattice parameter distances (here abusively called bond lengths) are denoted by $R_0(S_i, S_j)$ and depend on the bond type as well. We denote by $A_{ij}(S_i, S_j)$ [$B_{ik}(S_i, S_k)$] the local bond stiffness for nn (nnn) bonds, describing the energy cost of the bond length being different from its ideal value $R_0(S_i, S_j)$ [$R'_0(S_i, S_k)$], and by $r_{ij} = \|\vec{r}_i - \vec{r}_j\|$ (r_{ik}) the instantaneous distance between two nn (nnn) nodes. The expressions for the elastic stiffness of the nn and the nnn bonds are written under the following forms so as to decrease the total elastic constant in the HS spin state:

$$A_{ij}(r_{ij}) = A_0 + A_1 (r_{ij} - R_{\text{HS}}^0)^2 \text{ and } B_{ik}(r_{ik}) = B_0 + B_1 (r_{ik} - \sqrt{2} R_{\text{HS}}^0)^2, \quad (2)$$

where A_0 (B_0) and A_1 (B_1) are, respectively, the harmonic and the anharmonic contributions to the elastic interaction energy between nn (nnn) neighbors. In the Hamiltonian (1), the surface sites are kept invariant in a HS state as a result of the weakening of the ligand field at the surface of the SC nanoparticles.

Realistic transition temperatures are obtained with an energy gap $\Delta = 900$ K and the degeneracy ratio g , such as $\ln g \approx 10$ yielding an electronic entropy change at the transition $\Delta S = N k_B \ln g \approx 82 \text{ JK}^{-1} \text{ Mol}^{-1}$ and a transition temperature $T_{\text{eq}} = \Delta / k_B \ln g \approx 90$ K in the case of pure Ising-like model.^{36,37} The equilibrium lattice parameters for the three spin configurations, derived from x-ray data,¹⁹ are $R_0(-1, -1) \approx 1$ nm, $R_0(+1, +1) \approx 1.2$ nm, and $R_0(+1, -1) \approx 1.1$ nm. We set the average value of the lattice parameter between nnn neighboring HS (LS) atoms as equal to $\sqrt{2} \times R_0(S_i, S_j)$. The elastic constants A_0 and A_1 (B_0 and B_1) between nn (nnn) sites are derived from the experimental bulk modulus, $E \approx 1\text{--}10$ GPa,⁴⁴ which leads to $A_0 \cong 4000 \text{ K/nm}^2 \approx 4 \text{ meV/\AA}^2$ and we set the nnn elastic interaction $A_1 = 0.4 \text{ meV/\AA}^4$ ($B_0 = A_0$ and $B_1 = A_1$). Using these parameter values, the elastic constants of HS and LS states are, respectively, $A(+1, +1) = 4 \text{ meV/\AA}^2$ and $A(-1, -1) = 8 \text{ meV/\AA}^2$, and we choose for the mixture HS and LS,

which is much less well defined, an elastic constant equal to the arithmetic mean value of that of the HS and LS states, $A(+1, -1) = 6 \text{ meV/\AA}^2$ [we have fixed $B(+1, -1) = A(+1, -1)$].

A. Structure of the electroelastic Hamiltonian and its relation with the Ising-like Hamiltonian

We investigate in this section the relation between the Hamiltonian (1) and the usual Ising-like Hamiltonian,^{35–37} which was widely studied in the literature. To make the things simple, we study the structure of Hamiltonian (1) in the case of a harmonic interaction, i.e., $A = A_0$, and we restrict the elastic interaction to the first nearest neighbors. The nnn interaction, appearing in the third term of Eq. (1), is not included. We also forget about the constraint imposed to the surface. Then Eq. (1) becomes

$$H = \sum_i \frac{1}{2} [\Delta - k_B T \ln(g)] S_i + \sum_{(i,j)} A_0 [r_{ij} - R_0(S_i, S_j)]^2. \quad (3)$$

The spin-spin interaction in the Hamiltonian (3) comes from the elastic contribution in which the equilibrium distance between two neighbors depends on their spin states. It is quite easy to remark that the equilibrium distance $R_0(S_i, S_j)$ can be expressed as a function of the spin variables as

$$R_0(S_i, S_j) = \rho_0 + \rho_1 (S_i + S_j) + \rho_2 S_i S_j, \quad (4)$$

where the quantities, ρ_0 , ρ_1 , and ρ_2 are obtained as a function of the nn equilibrium distances $R_0^{\text{HH}} = R_0(+1, +1)$, $R_0^{\text{LL}} = R_0(-1, -1)$, and $R_0^{\text{HL}} = R_0(+1, -1) = R_0^{\text{LH}} = R_0(-1, +1)$, as follows:

$$\rho_0 = \frac{1}{4} (R_0^{\text{HH}} + 2R_0^{\text{HL}} + R_0^{\text{LL}}); \rho_1 = \frac{1}{4} (R_0^{\text{HH}} - R_0^{\text{LL}}), \text{ and} \\ \rho_2 = \frac{1}{4} (R_0^{\text{HH}} - 2R_0^{\text{HL}} + R_0^{\text{LL}}), \quad (5)$$

where R_0^{HH} , R_0^{LL} and R_0^{HL} are the equilibrium nn distances between HS-HS, LS-LS and HS-LS atoms, respectively.

In the calculations, we have considered $R_0^{\text{HL}} = \frac{1}{2} (R_0^{\text{HH}} + R_0^{\text{LL}})$ and then we have $\rho_2 = 0$. One can remark that ρ_0 is the average value of the equilibrium distance over the fourth spin configurations of two neighbors, while $4\rho_1$ is the lattice parameter misfit between the LS and the HS phases. Inserting the expression (5) into Eq. (1) and after some simple mathematical developments, one can arrive to the following general Ising-like Hamiltonian with local exchange-like interaction J_{ij} and field-like h_i :

$$H = \sum_{(i,j)} J_{ij} S_i S_j + \sum_i h_i S_i + \frac{A_0}{2} \sum_{(i,j)} (r_{ij} - \rho_0)^2 + \frac{zN}{2} A_0 \rho_1^2, \quad (6)$$

where, J_{ij} and h_i are given by

$$J_{ij} = A_0 \rho_1^2 \text{ and } h_i = \frac{1}{2} (\Delta - k_B T \ln g) - A_0 \rho_1 \sum_{j=1}^z (r_{ij} - \rho_0). \quad (7)$$

Equation (7) allows a direct identification of the exchange-like interaction J as the elastic energy associated with the volume change (or the volume misfit) between the LS and the HS states. This model establishes a direct relation between the phenomenological interaction parameter J , of the widely used Ising-like model and the elastic energy of the volume misfit, $A_0\rho_1^2$, thus demonstrating the elastic nature of the parameter J . Moreover, the short-range interaction J is a positive quantity, which means that it stabilizes HS-LS configurations. This is in excellent agreement with general elasticity theory, which predicts repulsive interactions between nearest neighbors via short-wavelength or optical phonons. Indeed, from the elastic point of view, when one puts a large HS ion at a certain site, it pushes apart the surrounding metals, and so it is more favorable to have small LS ions at the nn sites. The field-like contribution h_i contains the combined synergetic effects of the temperature-dependent energy gap, $\frac{1}{2}(\Delta - k_B T \ln g)$, and those of the local elastic field produced by the neighbors, where both of them stabilize the HS (LS) state at high (low) temperature.

Based on the previous analysis developed on Ising-like models,³⁷ the transition temperature T_{eq} is found as the temperature for which $\langle h_i \rangle = 0$, which gives $T_{\text{eq}} = \frac{\Delta}{k_B \ln g}$. Moreover, the system undergoes a first-order phase transition when $T_{\text{eq}} < A_0\rho_1^2$.

One can wonder in the present study if the well-known Mermin-Wagner theorem,⁴⁵ which excludes an ordered state for a continuously degenerate 2D system at finite temperatures,⁴⁶ is violated. In fact, Mermin-Wagner theorem has some prerequisites that are not satisfied in the present situation. In particular, it is not relevant for the case of nanoparticles problem, since the system is far from the thermodynamic limit and infrared divergence of the correlation function plays no role. Moreover, we would like to notice that, in the presence of a dipole interaction, which decreases with distance r as r^{-3} , already another prerequisite of this theorem is not fulfilled, namely, a short-range interaction $\propto r^{-\alpha}$ with $\alpha \geq 2D$, where D refers to the spatial dimension.⁴⁷ Therefore 2D ferromagnets and antiferromagnets exhibit a collectively ordered state with a critical temperature of the order of the exchange interaction J provided that, for example, dipole coupling is present even if this interaction is weak compared to J .⁴⁸ In the present problem, integrating out the phonons introduces a long-range interaction.

III. RESULTS AND DISCUSSION

Hamiltonian (1) cannot be solved analytically so we perform MC simulations to study its thermal properties (hysteresis, transition temperature, and residual fraction) for systems sizes $L = 6, 10, 18, 40,$ and 60 . For simplicity reasons, we will not consider here the distribution of nanoparticles sizes arising from the synthesis. Our objective is to understand how the nanoparticle size impacts its thermodynamic properties. In practice, the system is warmed up from $T = 50$ to 250 K in steps of increment 1 K, and then cooled down to the initial temperature 50 K. The MC procedure was performed in the following way: for a single particle, randomly selected, of type $S_i (= \pm 1)$ and at position \vec{r}_i , we chose a new value $S'_i (= -S_i)$ at fixed lattice positions. This random change is accepted or rejected by the usual Metropolis criterion. When

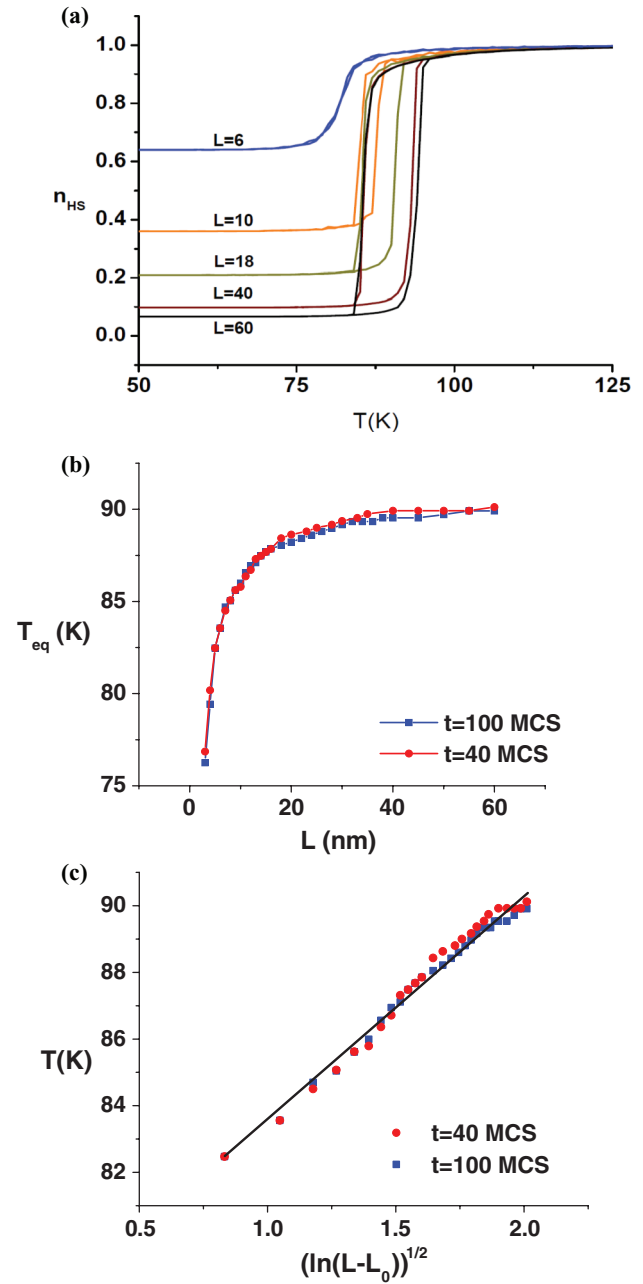


FIG. 2. (Color online) (a) Thermal dependence of the HS fraction for square-shaped nanoparticles of different sizes L . The simulations have been performed with a temperature sweep rate of 0.01K/MCS . (b) The size dependence of the transition temperature showing a drastic change below $L \approx 20$ nm. Red and blue points correspond to two different temperature sweep rates, 0.025 ($t = 40$ MCS) and 0.01 ($t = 100$ MCS) K/MCS, respectively. (c) The universal behavior of the transition temperature with size showing a logarithmic behavior.

the random spin change is accepted, we then move the lattice by choosing randomly a position r_j , which is slightly moved from its position keeping the other particles positions and spins fixed. We then visit sequentially the N lattice positions until we relax the lattice. In the next step, we chose again randomly a new spin variable and the procedure is repeated for all the N lattice nodes.

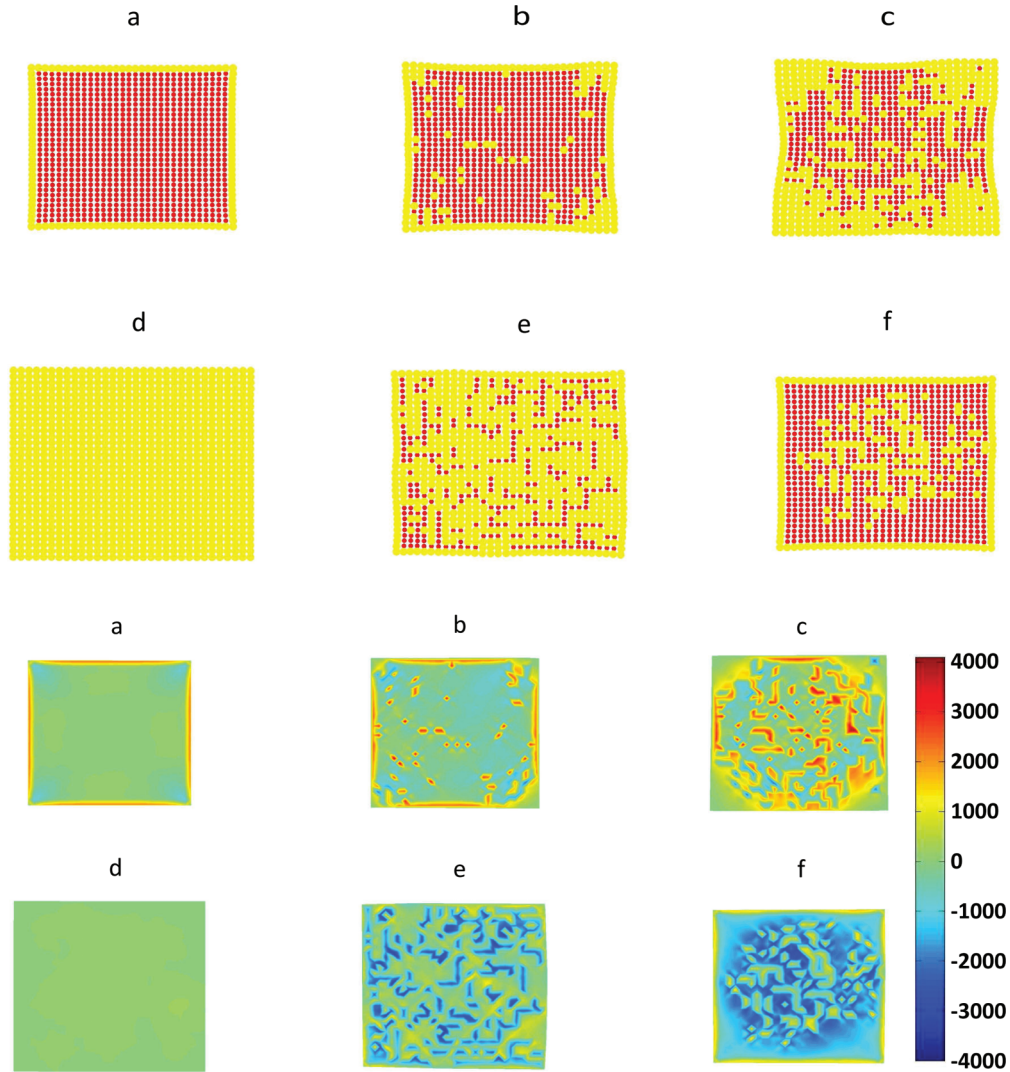


FIG. 3. (Color online) (Top) Snapshots of the system from low to high temperatures. The red (yellow) dots are associated with LS (HS) sites, while symbols a, b, c, d, e, and f are related with the respective temperatures 5, 95, 100, 144, 86, and 80 K. (Bottom) Corresponding snapshots of the distribution of local pressures.

At each temperature, 100 MC steps are used to relax the spin configuration, and for each spin change $100 \times N$ lattice positions to relax the lattice deformations. In addition, at each temperature, 100 MC steps on the spin configuration are discarded as transient time and the subsequent 100 MC steps were used to measure the following physical quantities:

$$\langle S \rangle = \frac{4(L-1) + \sum_{i=1}^{(L-2)^2} S_i}{L^2} \text{ and } n_{\text{HS}} = \frac{1 + \langle S \rangle}{2}, \quad (8)$$

where $\langle S \rangle$ is the average value of the spin and n_{HS} is the HS fraction, i.e., the fraction of SC molecules in the HS state.

A. Case of one HS layer at the surface

In Fig. 2(a), we show the thermal behavior of the HS fraction, $n_{\text{HS}}(T)$, calculated for various particle sizes, corresponding to the case of Fig. 1(a). The experimental behaviors^{30,31} are reproduced: upon decreasing particle size, the transition temperature is downward shifted, the hysteresis loop progressively collapses and the low-temperature residual

HS fraction is increased. Indeed, the HS fraction n_{HS} exactly follows the shell/core atom ratio, which is simply expressed as $\frac{4(L-1)}{L^2}$, with an asymptotic regime $\approx 4/L$ for large nanoparticle sizes. Figure 2(b) shows the size dependence of the transition temperature for various nanoparticle sizes.

The transition temperature determined for various sizes is shown in Fig. 2(b). Its behavior is less obvious than that of the residual fraction. Indeed, the size dependence of T_{eq} involves local ligand contributions due to the constraint imposed on the surface atoms. In addition, the dependence of the Hamiltonian on space variables makes the problem less trivial and its analytic investigation as performed in Ref. 29 is no more possible. Thus, due to the presence of long-range elastic interactions, the shape $T_{\text{eq}}(L)$ is different from that derived from an adapted Ising-like model²⁹ for nanoparticles. We have found that the size dependence of the transition temperature, shown in Fig. 2(b), follows the universal law

$$T_{\text{eq}}(L) = 76.3 + 7.1\sqrt{\ln(L - L_0)}, \quad (9)$$

where $L_0 = 3$ is the smallest size from which the system can convert from LS to HS. The relation (9) reproduces very well the data of the simulations, as shown in Fig. 2(c). It is also in excellent agreement with recent experimental data on SC nanoparticles,³¹ which reported a logarithmic behavior for the transition temperature with size. However, it should be remarked that Eq. (9) has a strong limitation when we approach the bulk behavior at which the transition temperature must saturate. Therefore it must be restricted to a region in which the nanoparticle behavior strongly depends on its size.

Figure 3 gives evidence for domain growth starting from all corners where the edge atoms are constrained to keep the high-spin (HS) state with $L = 30$, both for the HS \rightarrow LS and the LS \rightarrow HS processes. The domains propagate towards the center of the crystal and then collapse. These results are in good agreement with previous molecular-dynamics (MD) and MC studies,^{49,50} obtained on nonconstrained surface systems. The maps of local pressures are shown in line 2 of Fig. 3 for a system changing from HS (LS) to LS (HS) states. There, we find an inhomogeneous distribution of positive (negative) pressure, which is due to the shrinking (expansion) of molecules. Such inhomogeneous structure has been found in a domain-wall propagation experiment.⁵¹

As a result of the fixed HS surface, the neighbouring active atoms feel an additional elastic contribution X to the effective-field-like h given in Eq. (7), the expression of which reads

$$X = \frac{1}{2} A_{ij} \left[r_{ij} - \frac{R_0(+1, +1) + R_0(-1, -1)}{2} \right]^2 - \frac{1}{8} A_{ij} [R_0(+1, +1) - R_0(-1, -1)] \times \left[r_{ij} - \frac{R_0(+1, +1) + R_0(-1, -1)}{2} \right], \quad (10)$$

where $A_{i,j} = A_0 + A_1[r_{ij} - R_0(+1, +1)]^2$. Since $r_{ij} \leq R_0(+1, +1)$, the contribution obtained in Eq. (10) that acts as a negative pressure, which stabilizes the HS state, results in a decreasing transition temperature with size, as observed in Fig. 2(b). In addition, this contribution is enhanced at small sizes due to the increase of the surface/volume ratio. These behaviors reproduce quite well the experimental magnetic data reported in literature of SC nanoparticles,^{30,33} and also explained using an Ising-like model. Moreover, very recent studies³⁸ on the matrix-dependent cooperativity in SC Fe(pyrazine){Pt(CN)₄} nanoparticles obtained from the microemulsion for which their washing by adding *para*-Nitrobenzyl pyridine (*p*Nbp) up to the complete removal of the organic matter results in very similar observations as those predicted by the present model.

In our results, the transition temperature exists from $L = 3$, and its behavior for larger sizes is almost independent on the temperature sweep rate as seen in Fig. 5(a), where we reported the results for two different temperature scan rates, 0.025 and 0.01 K/MCS corresponding to the respective MC waiting times of 40 and 100 MCS, between two increments of temperature.

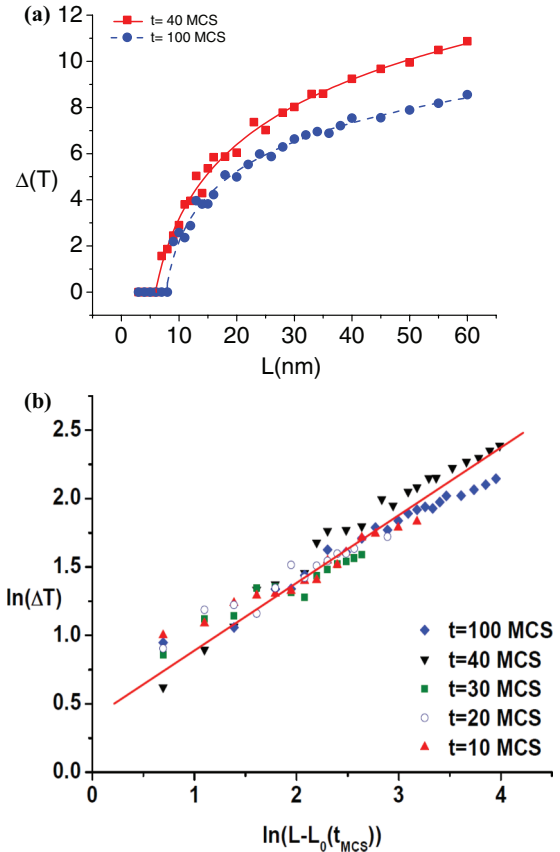


FIG. 4. (Color online) (a) Size dependence of the thermal hysteresis width of the SC nanoparticle in the frame of the elastic model of Hamiltonian (3), showing the existence of a threshold size L_0 for the occurrence of the thermal bistability. The curve with red squares (blue filled circles) for which $L_0 = 6$ ($L_0 = 9$) corresponds to a temperature sweep rate of 0.025 K/MCS (0.01 K/MCS). (b) Universal behavior of the hysteresis with size. The data result from different MC kinetics corresponding to different MC waiting time between two temperatures during the simulations. All curves match on the same universal linear plot with a slope of value $\frac{1}{2}$. The threshold value L_0 depends on the MC kinetics.

B. The size dependence of the hysteresis loop

According to Figs. 2(a) and 4(a), the hysteresis loop appears above a threshold value. Obviously, this value depends on the temperature scan rate used in the simulation. Therefore we have calculated [see Fig. 5(a)] the size dependence of the hysteresis width for two temperature scan rates of 0.025 and 0.01 K/MCS. On increasing L , above the respective critical values, $L_c \approx 5$ and 8 nm, the hysteresis width ΔT shows a monotonous increase with size until an asymptotic value $\Delta T \approx 12$ K obtained for large lattice size values ($L \approx 100$ nm for 0.025 K/MCS). This monotonic behavior contrasts with the nonmonotonic one depicted by the Ising-like model²⁹ with a fixed HS border. Indeed, in the former, the hysteresis width goes through a maximum when decreasing the size, a behavior which has been attributed to the HS surface, which acts as a nonuniform negative pressure. Although this negative “pressure” exists in the present model, its amplitude remains quite small (~ 10 K). Additionally, while the interaction is exclusively short ranged in the case of Ising-like model, here

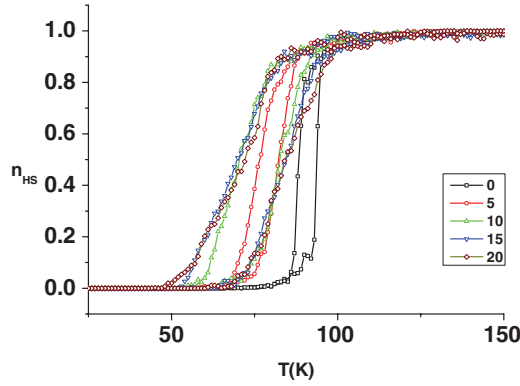


FIG. 5. (Color online) Thermal dependence of the HS fraction for square-shaped nanoparticles at constant core size $L = 10$ surrounded by a various number of HS shell layers. The hysteresis shifts downwards as a result of the negative elastic pressure induces by the shell.

the long-range elastic interaction hinders the presence of this nonmonotonous behavior of the hysteresis width. In fact, a similar behavior is also obtained in the Ising-like model when we added a long-range interaction between the nanoparticles,²⁹ which makes the present results very consistent.

Figure 4(b) shows the size dependence of the hysteresis loop for different MC scan rates at which we have evaluated for each case the threshold value of size, denoted by L_0 . Remarkably, we have found that the hysteresis width ΔT follows the simple law

$$\Delta T(L, t_{\text{MCS}}) \propto [L - L_0(t_{\text{MCS}})]^{\frac{1}{2}}. \quad (11)$$

In Eq. (11), t_{MCS} is the MC waiting time between two consecutive temperature measurements (here, $\Delta T = 1$ K). We should mention that the universal behavior presented in Fig. 4(b) is only valid for small size nanoparticles. Indeed, at bigger sizes, the hysteresis width reaches the bulk value at which it saturates and Eq. (10) is no longer valid.

IV. THE CORE/SHELL PROBLEM

In this section, we study the particular and interesting case of core-shell SC nanoparticles. For simplicity reasons, the studied particles are square-shaped and have a 2D character. The core shell nanoparticle contains a core part, which is constituted by active atoms (which may have HS or LS states), and its size is fixed here to $L = 10$. The shell is made of several layers of inactive atoms covering the core of the nanoparticle. From the structural point of view, we study here the effect of the shell size on the thermal properties of the HS fraction. The elastic constant between the shell atoms is that of the HS state in order to mimic the effect of a soft shell. We stress on the fact that since the shell atoms are electronically inactive, the shell effects are purely elastic. We should mention that the study of the shell size cannot be investigated in our previous Ising-like model²⁹ designed for SC nanoparticles. The reason is that increasing the number of HS layers at the surface does not change anything in the model, which includes only short-range electronic interactions between active spins, and therefore the thermodynamic properties of the system with one HS layer and several HS layers are the same. This drastic limitation comes

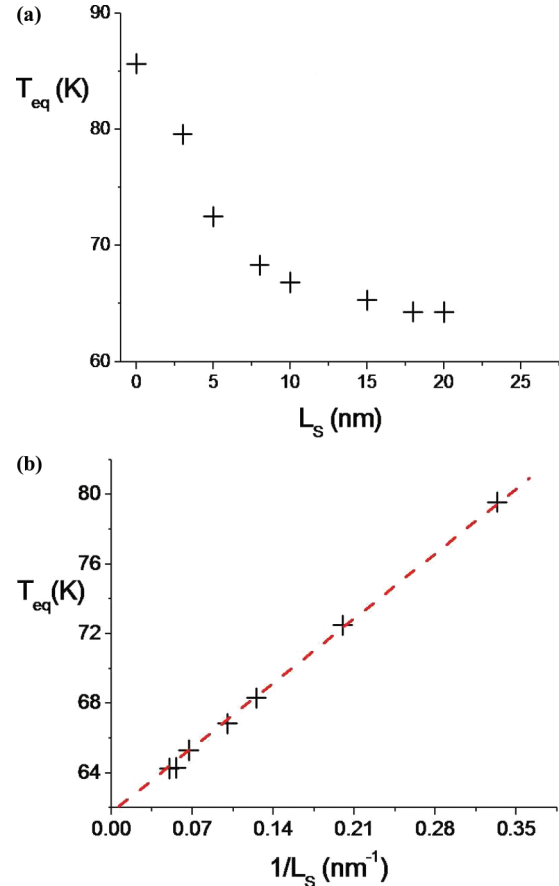


FIG. 6. (Color online) (a) The HS shell size dependence of the equilibrium temperature. (b) T_{eq} vs $1/L$ showing a linear behavior.

from the fact that the Ising-like model does not include the elastic interactions.

A. Equilibrium properties

The thermal dependence of the HS fraction for different shell sizes is presented in Fig. 5. We see that contrary to the case of Fig. 2(a), the high-spin fraction is shifted towards lower temperatures with increasing dimensions of the shell for a fixed core size, $L = 10$. This tendency confirms the existence of a negative elastic pressure exerted by the shell part on the core, which leads to the increase of the width of the hysteresis loop. This negative strain is an internal pressure of elastic origin. The core of the nanoparticle, embedded in a soft matrix (the shell), has a bigger lattice parameter, as a result of the soft elastic constants of the “matrix.” An inspection of the transition temperature for the different HS shell sizes, presented in Fig. 6(a), shows that the latter is inversely proportional [see Fig. 6(b)] to the size L_S of the HS shell.

In the next step, we have analyzed the effect of the shell size on the nucleation and growth of the HS fraction associated with the hysteresis of Fig. 5. The results are summarized in Fig. 7, where we depict the spatial distribution of the HS fraction, upon the thermal SC transition in the case of a free surface nanoparticle and a core-shell nanoparticle. The first case resembles that of a one HS layer at the surface and shows the appearance of HS domains upon heating. Upon increasing

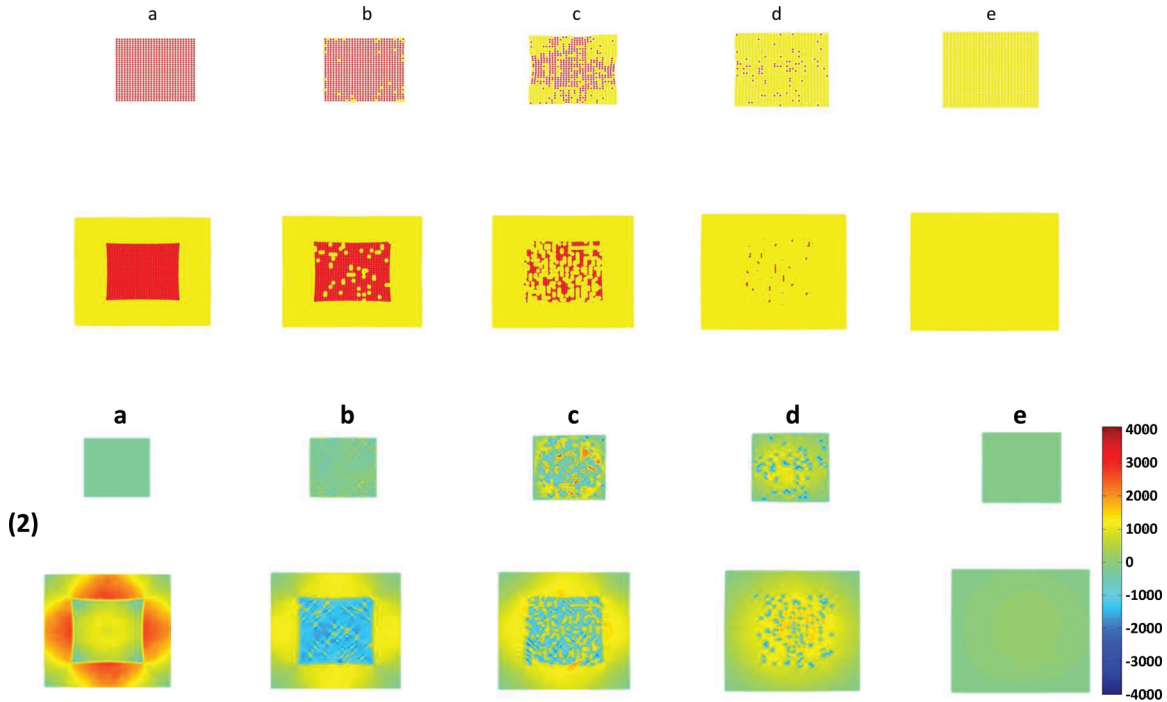


FIG. 7. (Color online) (1) Snapshots of the spin configuration during the thermal transition from LS to HS state, where the HS (LS) sites are represented by the yellow (red) dots. Top (down) figures correspond to nanoparticles without (with) a HS shell of size $L_s = 10$. The shell hinders the single domain growth process. (2) Corresponding snapshots of the spatial distribution of local pressures upon heating for the same lattices. For core shell nanoparticles, we remark the existence of negative pressures around the corners of the core part. Symbols a, b, c, d, and e correspond to temperatures 5, 85, 96, 106, and 173 K, respectively.

the core shell width L_s , we found the existence of a threshold value of L_s at which the shell hinders the formation of the HS domains upon heating. Although the SC transition is of first order, as seen in Fig. 5 for the value $L_s = 10$, the transition between the LS and the HS states takes place through ramified domains structure. This result reminds that of elastic systems with periodic boundary conditions,⁴⁰ where surface effects are absent. In fact, the ultimate case where the shell width is infinite leads to the situation of a nanoparticle embedded in a matrix. This limiting case has been studied recently by other authors,²⁸ but the effect of the matrix size has never been addressed. In Fig. 7, we represent the spatial distribution of local pressures corresponding to the electronic configurations of Fig. 5. A comparison between the free surface and core-shell system shows the existence of a negative local pressure mainly distributed around the corners. Around the edges, a positive pressure is observed, and inside the lattice the local pressure is almost negligible in the LS state, while it is positive in the HS state, due to the volume expansion of the core of the nanoparticle.

B. Nonequilibrium properties

Now we study the relaxation properties of the core-shell SC nanoparticles in order to investigate the effect of the elastic stress induced by the shell on the relaxation properties of the nanoparticle as a function of the size of the HS shell. Equilibrium properties, presented in Fig. 5, have shown that the effect of a soft shell on the nanoparticle stabilizes the

HS state, since the transition temperature is lowered. The study of the relaxation of the HS fraction is a little bit more subtle, because the system contains lattice and spin degrees of freedom, and then the results are very sensitive to the preparation of the initial state. Usually, in SC systems, the metastable HS state at low temperature can result from two kinds of preparations: (i) by light through the light-induced excited spin state trapping (LIESST)¹⁵ or by (ii) a rapid thermal quenching from the high temperature state.^{52,53} In the case of the photoexcitation process, the induced HS state (produced at ~ 10 K) obeys the Franck-Condon principle.^{44,54} The latter is the approximation that an electronic transition is most likely to occur without changes in the positions of the nuclei in the molecular entity and its environment. The resulting state is called a Franck-Condon state, and the transition involved, is a vertical transition. In our case, these instantaneous electronic transitions allow to transform the spin state of the atoms from LS to HS at frozen lattice positions of the LS lattice. In contrast, in the case of thermally quenched systems, the initial state is made of HS atoms with the lattice positions associated with those of the HS state (i.e., containing the thermal disorder arising from the thermal fluctuations). Here, for practical reasons, we restrict ourselves to the study of the relaxation of photo-induced HS states. We investigate the relaxation of the photoinduced HS state in two steps: (i) first, we look for the mechanical equilibrium of the nanoparticle before photoexcitation at low temperature, and (ii) we change all the spins of the core to HS by keeping the distances and we relax electronically and elastically the obtained lattice.

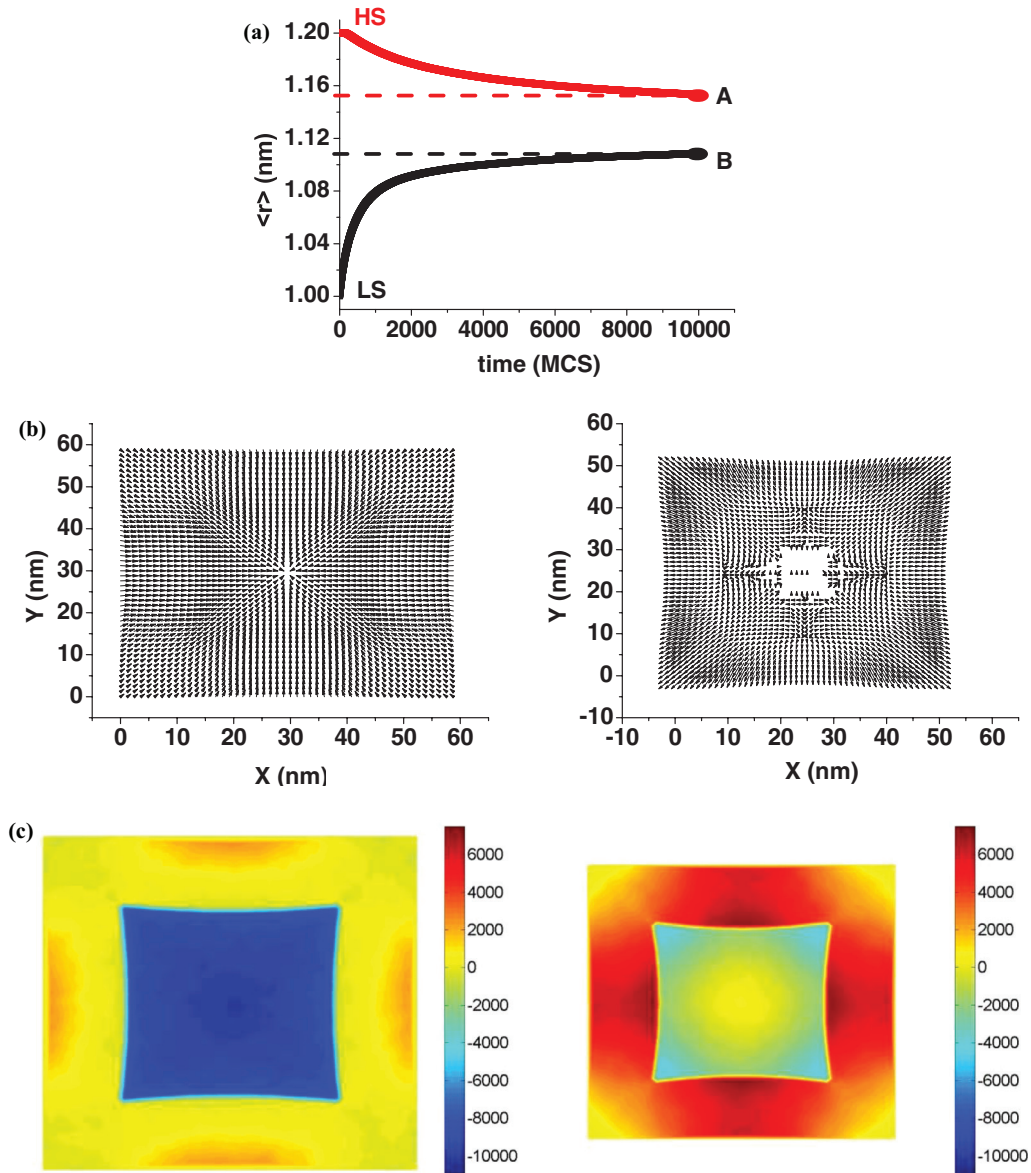


FIG. 8. (Color online) (a) Time dependence of the average value $\langle r \rangle$ of the lattice parameter during the elastic relaxation of a core shell nanoparticle for a frozen electronic state. The red (black) curve corresponds to the elastic relaxation from an initial structure with a HS (LS) lattice parameter value. (b1) and (b2) are the respective corresponding displacement fields at mechanical equilibrium points A and B of (a). (c1) and (c2) are the spatial distributions of the strain in the lattice at points A and B of (a).

1. The structure optimization

Another difficulty arising from the specific nature of core-shell nanoparticles is the determination of the elastic structure at mechanical equilibrium of the nanoparticle, before the photoexcitation. Indeed, at low temperature, the nanoparticle is made of a core with an LS lattice parameter surrounded by a shell which has a different lattice parameter. It is not obvious how to build up geometrically such a lattice because of the existence of a lattice misfit, which leads to incommensurate surfaces between the core and the shell. To avoid such complications, we have studied the relaxed elastic state of LS nanoparticles starting from two cases, where all atomic distances are equal to R_0^{LL} or to R_0^{HH} . The elastic relaxation of the nanoparticle for these two initial states is represented in Fig. 8(a), where

we have plotted the time dependence of the average atomic distance. Interestingly, the relaxed mechanical state of the system depends on the initial lattice structure. To visualize spatially the elastic properties of the lattice, we show in Fig. 8(b) the spatial distribution of the displacement field corresponding to the final states of Fig. 8(a), and we depict in Fig. 8(c) the associated distributions of the internal strain. The internal pressure at site i is obtained through the following relation:

$$P_i = - \sum_j A_{ij} [r_{ij} - R_0(S_i, S_j)] - \sum_k B_{ik} [r_{ik} - R_0(S_i, S_k)], \quad (12)$$

where j and k run over the nearest and the next-nearest neighbors of the site i , respectively.

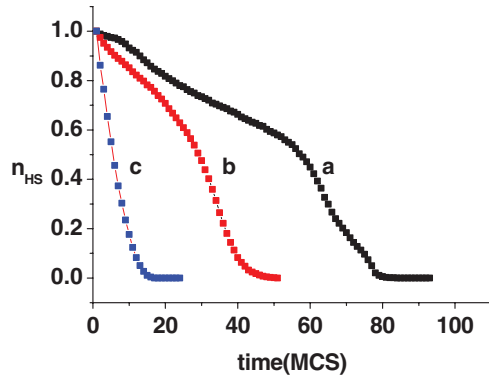


FIG. 9. (Color online) Time dependence of the normalized HS fraction during the relaxation from the metastable HS to LS states. (a) The case of shell-free nanoparticle. (b) Corresponds to the case of a core shell nanoparticle with the initial state A of Fig. 8. Curve (c) depicts the relaxation of core shell nanoparticle starting for the initial state B of Fig. 8(a). The cases b and c demonstrate that the soft shell leads to a decrease in the lifetime of the HS metastable state through the relaxation of its elastic strain. The dimensions of the core and the shell are the same as those of Fig. 8.

The examination of the spatial distribution of the displacement field, given in Fig. 8, shows that in the case of a nanoparticle having initially an HS lattice parameter [red curve of Fig. 8(a)], a global contraction of the lattice takes place [see Fig. 8(b1)]. The associated spatial distribution of the strain over the lattice [see Fig. 8(c)] indicates the existence of a weak positive pressure at the surface of the lattice and almost no strain in the shell, while a strong tensile stress is present in the core part of the nanoparticle, which is electronically LS. These results can be well understood since the core of the nanoparticle wants to shrink, but it is hindered by the shell, which wants to keep the structure in the HS state. So an agreement is found between the two structures that minimize the elastic energy associated with the elastic misfit. In contrast, when the whole nanoparticle structure is initially prepared with an LS lattice parameter, a nonconventional lattice deformation field is obtained [see Fig. 8(b2)]. In such case, the shell wants to expand, while the core wants to keep the LS lattice parameter. The competition between these two antagonistic processes results in a nontrivial behavior of the displacement field, which shows the existence of vortices around four regions of the lattice situated in the shell part. The associated strain distribution clearly shows that the core is almost at equilibrium (the lattice strain is weak) while the shell is submitted to a strong compressive strain resulting from the choice of the initial structure. While one may expect just a symmetric behavior between the distributions of the strain fields of Fig. 8(c), fundamental differences are obtained in its spatial behavior. In particular, Fig. 8(c1) shows clearly that starting from the center lattice and going along its diagonal to reach the surface, the strain increases monotonously. In contrast, Fig. 8(c2) evidences that the strain field, which is almost zero in the center, first decreases when we reach the limit of the core, and finally it sizably increases in the shell region. Thus, in the case of Fig. 8(c2), the behavior of the strain is not monotonous along the space coordinates.

2. Relaxation of the HS fraction

Once the mechanical equilibrium state of the nanoparticle is defined, we can proceed to the study of the relaxation of its photoexcited state. Here, we study the relaxation of three photoexcited states built from the elastic initial state A and B of Fig. 8(a) (for the core shell). To emphasize the role of the shell in the nanoparticles, we also investigate the relaxation of a photoexcited state of a free-shell nanoparticle having the same size 30×30 as that of the core considered in Fig 8(a).

The photoexcited states are obtained by flipping the spin states of the nanoparticle's core from LS to HS and keeping the lattice positions invariant. This procedure intends to mimic the light excitation, which results in the Franck-Condon process that changes the electronic state of SC metal at fixed nuclear coordinates. We have studied the relaxation of the three types of HS states at 10 K for nanoparticles having the same size, 30×30 , of the active part (the core). The relaxation curves are shown in Fig. 9 for these two cases. It is observed that both relaxation curves show a sigmoidal shape, indicating that the relaxation process is cooperative. In contrast, it is easy to see that the nanoparticles with the shell (curves (b) and (c)) relaxes faster than the shell-free one (curve (a)). To understand this result, it is important to see that the initial state of the nanoparticle with a shell is an LS core and an HS shell, where the shell (the core) experiences a compressive (tensile) stress, as clearly depicted in Fig. 7. After photoexcitation, we transform the LS spin sites of the core in the HS state and then the core part wants to expand, but the shell cannot absorb all the volume change and therefore a compressive stress appears on the core part of the nanoparticle, as the one obtained in the thermally induced HS state of Fig. 7. This compressive stress acts as a nonuniform pressure on the metastable HS, thus reducing its lifetime, as depicted in Fig. 9. This result is in excellent agreement with recent experimental observations⁵⁵ obtained on core-shell nanoparticles of photomagnetic Prussian Blue analogs (PBA) in which the shell part has a smaller rigidity. We have also considered the relaxation of the HS thermally quenched state. For that, we fixed the initial HS state to that of the high-temperature state obtained in Fig. 7. An interesting aspect of this state is the presence of local fluctuations in the atomic bond lengths. The corresponding relaxation curve, given in Fig. 8(c), has also a shorter lifetime than that of the free shell nanoparticle due to the presence of a residual compressive stress induced by the shell on the core.

V. DISCUSSION AND CONCLUSION

We have investigated the thermal properties of SC nanoparticles mainly from the point of view of the size dependence of their hysteresis loop. It is well known that the width of the hysteresis is related to the observation time and to the ratio of the barrier height to the thermal energy $k_B T$. We found the existence of a universal law linking the hysteresis width with the size of the nanoparticle for various temperature sweep rates. Among the results presented in this manuscript, we focus on the important difference of the size dependence of the core and the shell of the nanoparticle. For simplicity, we assumed that the shell has the same elastic properties as those

of the HS state. However, in real systems, the situation can be much more complicated, and although the surface atoms are most likely in the HS state, the ligand field increases gradually from the surface to the bulk up to that of the nanoparticle's core. Due to large uncertainties on the space dependence of the ligand field, we preferred to investigate limiting situations where the surface atoms are in the HS state, due to their coordination to water molecules. We have also considered the special case of core-shell SC nanoparticles, a problem which was not yet investigated theoretically. To take into account the elastic misfit between the core and the shell, we have considered that the latter has the same elastic constant as that of the HS state. Obviously, considering softer shells is very easy to include in the model, but the present situation already clarifies the role of the shell. Indeed, our calculations have shown that competing effects take place between the core and the shell of SC nanoparticles allowing to explain the various experimental data of literature, where it has been observed that, in some cases, the hysteresis shifts downwards when decreasing the size of nanoparticles, while in some other cases the hysteresis remains almost unaffected³⁴ by the changes of the particle size. From the theoretical point of view, shell-free nanoparticles lead to hysteresis widths the size of which decreases with their size. However, when we take into account surface effects, from the electronic point of view (as reported in Ref. 29) or through some specific elastic properties at the surface, then new behaviors may emerge. That is the case, for example, when we consider an SC nanoparticle surrounded by a shell that has a softer bulk modulus than that of the core. In this case, the increase of the shell size increases the hysteresis loop, which shifts downwards. In real systems, an increase of the nanoparticle size leads to a simultaneous increase of the shell and active core size, and therefore the two previously mentioned effects can compete and give rise to a size-independent thermal hysteresis, as already reported in some previous experimental works.³⁴ This very interesting aspect of the present model will be investigated in a separate work.

Although, we have not studied the dependence of the energy barrier with size, it is expected that the latter decreases with size, as recently reported in circular lattices.³⁸ However, in the present study, its determination requires the time dependence of the HS fraction at different temperatures and, hence, its derivation from an Arrhenius plot. Simple arguments lead, however, to expect that the true experimental situation is much more complicated. Indeed, the hysteresis width depends on the energy barrier, which itself may scale with the volume of the system, but the latter also depends on the interface between the nanoparticle and its immediate environment. Actually, the change in the composition of the nanoparticle surface results in a large shift in the center of the hysteresis.

This effect indicates that the interface energy determines the thermodynamic transition point. Here, the interface energy most likely involves the breaking or rearrangement, or both, of bonds between surface atoms and organic ligands (or water molecules) and depends on the type ligands used. It is worth mentioning that the previous trends on the energy barrier do not extrapolate to the bulk solids, where usually barrier heights are lower than in nanocrystals, mainly because of the influence of defects. For example, the hysteresis width of the transition from wurtzite to rock salt in bulk CdSe (a transition which is accompanied by a structure change) is approximately one-third of the width observed in CdSe nanocrystals.⁵⁶ Moreover, the stability of the bulk structure for small particles is questionable. For example, it is quite known that small nanoparticles of Co-Pt bimetallic clusters have different stable structures, depending on their size. Thus global optimization MC simulations,⁵⁷ based on tight-binding potentials, have shown in this particular case that polyicosahedronlike, decahedron, and fcc structures are the most stable for nanoparticles with atom numbers $N < 100$, $100 < N < 400$, and $400 < N < 1000$, respectively. In addition, real nanoparticle materials, involve surface relaxation and surface reconstructions, which may play the role of active point defects for nucleation during the SC transition. At the present stage, we have no x-ray diffraction data on SC nanoparticles due to the difficulty to perform high-quality experiments, mainly because of the presence of structural disorder at the surface and, probably, in the bulk of these molecular materials. Therefore the models constructed from highly symmetric lattices remain quite fragile and global structural optimizations will be unavoidable in the future to treat in a realistic way the switchable nanoparticles. Moreover, the presence of surface defects may be also at the origin of the distorted shape of the experimental hysteresis loops reported in literature. The present model allows extensions on structure optimization after adding some physical ingredients on the interaction potential and can also include the double distribution of random elastic constants and random ligand fields for the surface atoms. We are presently investigating these effects as well as those related with the size distributions of the nanoparticles and their effect on the thermal hysteresis width.

ACKNOWLEDGMENTS

The present work has been supported by the University of Versailles and CNRS. The authors are indebted to F. Varret, E. Coronado, and J. A. Real for helpful discussions on experimental data of SC nanoparticles. H.B. Would like to thank the "Ministère de l'Enseignement Supérieur et de la Recherche" of the Algerian Government for the financial support during his stay in GEMAC.

*Corresponding author: kbo@physique.uvsq.fr

¹E. König, *Struct. Bonding* **76**, 51 (1991).

²P. Gütllich, *Struct. Bonding* **44**, 83 (1981).

³S. Decurtins, P. Gütllich, C. P. Köhler, H. Spiering, and A. Hauser, *Chem. Phys. Lett.* **139**, 1 (1984).

⁴H. Toftlund, *Coord. Chem. Rev.* **94**, 67 (1989).

⁵C. P. Köhler, R. Jakobi, E. Meissner, L. Wiehl, H. Spiering, and P. Gütllich, *J. Phys. Chem. Solids* **51**, 239 (1990).

⁶O. Kahn, *Molecular Magnetism* (VCH, New York, 1993).

⁷J. Zarembowitch and O. Kahn, *New. J. Chem.* **15**, 181 (1991).

- ⁸O. Kahn, J. Kröber, and C. Jay, *Adv. Mater.* **4**, 718 (1992).
- ⁹O. Kahn and C. Jay-Martinez, *Science* **279**, 44 (1998).
- ¹⁰O. Kahn, *Curr. Opin. Solid State Mater. Sci.* **1**, 547 (1996).
- ¹¹R. Jacobi, H. Spiering, and P. Gütllich, *J. Phys. Chem. Solids* **53**, 267 (1992).
- ¹²K. Boukheddaden, J. Linares, E. Codjovi, F. Varret, V. Niel, and J. A. Real, *J. Appl. Phys.* **93**, 7103 (2003).
- ¹³J. Linares, E. Codjovi, and Y. Garcia, *Sensors* **12**, 4479 (2012).
- ¹⁴G. Molnár, V. Niel, J. A. Real, L. Dubrovinsky, A. Bousseksou, and J. Mc-Garvey, *J. Phys. Chem. B* **107**, 3149 (2003).
- ¹⁵S. Decurtins, P. Gütllich, C. P. Köhler, H. Spiering, and A. Hauser, *Chem. Phys. Lett.* **105**, 1 (1984).
- ¹⁶S. Decurtins, P. Gütllich, K. M. Hasselbach, A. Hauser, and H. Spiering, *Inorg. Chem.* **24**, 2174 (1985).
- ¹⁷A. Bousseksou, K. Boukheddaden, M. Goiran, C. Consejo, M. L. Boillot, and J. P. Tuchagues, *Phys. Rev. B* **65**, 172412 (2002).
- ¹⁸J. Krober, E. Codjovi, O. Kahn, F. Grolière, and C. Jay, *J. Am. Chem. Soc.* **115**, 9810 (1993).
- ¹⁹P. Gütllich, A. Hausser, and H. Spiering, *Angew. Chem., Int. Ed. Engl.* **33**, 2024 (1994).
- ²⁰B. Gallois, J. A. Real, C. Hauw, and J. Zarembowitch, *Inorg. Chem.* **29**, 1152 (1990).
- ²¹E. W. Müller, J. Ensling, H. Spiering, and P. Gütllich, *Inorg. Chem.* **22**, 2074 (1983).
- ²²G. Vos, R. A. Le Fèvre, R. A. G. de Graff, J. G. Haasnoot, and J. Reedijk, *J. Am. Chem. Soc.* **105**, 1682 (1983).
- ²³E. König, G. Ritter, S. K. Kulshreshtha, J. Waigel, and H. A. Goodwin, *Inorg. Chem.* **23**, 1896 (1984).
- ²⁴A. Bousseksou, G. Molnár, P. Demont, and J. Mengotto, *J. Mater. Chem.* **13**, 2069 (2003).
- ²⁵E. Coronado, J. R. Galán-Mascarós, M. Monrabal-Capilla, J. García-Martínez, and P. Pardo-Ibañez, *Adv. Mater.* **19**, 1359 (2007).
- ²⁶A. Rotaru, F. Varret, A. Gindulescu, J. Linares, A. Stancu, J. F. Létard, T. Forestier, and C. Etrillard, *Eur. Phys. J. B* **84**, 439 (2011).
- ²⁷T. Kawamoto and S. Abe, *Chem. Commun.* 3933 (2005).
- ²⁸L. Stoleriu, P. Chakraborty, A. Hauser, A. Stancu, and C. Enachescu, *Phys. Rev. B* **84**, 134102 (2011).
- ²⁹A. Muraoka, K. Boukheddaden, J. Linares, and F. Varret, *Phys. Rev. B* **84**, 054119 (2011).
- ³⁰F. Volatron, L. Catala, E. Rivière, A. Gloter, O. Stephan, and T. Mallah, *Inorg. Chem.* **47**, 6584 (2008).
- ³¹A. B. Gaspar, V. Martinez, I. Boldog, V. Ksenofontov, A. Bhattacharjee, P. Gütllich, and J. A. Real, *Chem. Mater.* **22**, 4271 (2010).
- ³²R. Claude, J. A. Real, J. Zarembowitch, O. Kahn, L. Ouahab, D. Grandjean, K. Boukheddaden, F. Varret, and A. Dworkin, *Inorg. Chem.* **29**, 4442 (1990).
- ³³I. Boldog, A. B. Gaspar, V. Martinez, P. Pardo-Ibañez, V. Ksenofontov, A. Bhattacharjee, P. Gütllich, and J. A. Real, *Angew. Chem., Int. Ed.* **47**, 6433 (2008).
- ³⁴F. Prins, M. M. Capila, E. A. Osorio, and E. Coronado, *Adv. Mater.* **23**, 1545 (2011).
- ³⁵J. Wanjflasz and R. Pick, *J. Phys. Colloq.* **32**, C1 (1971).
- ³⁶A. Bousseksou, J. Nasser, J. Linares, K. Boukheddaden, and F. Varret, *J. Phys.* **2**, 1381 (1992).
- ³⁷K. Boukheddaden, I. Shteto, B. Hôo, and F. Varret, *Phys. Rev. B* **62**, 14796 (2000).
- ³⁸R. Yousuf, F. Volatron, S. Moldovan, O. Ersen, V. Huc, C. Martini, F. Brisset, A. Gloter, O. Stéphan, A. Bousseksou, L. Catala, and T. Mallah, *Chem. Commun.* **47**, 11501 (2011).
- ³⁹M. Clemente-León, E. Coronado, Á. López-Muñoz, D. Repetto, L. Catala, and T. Mallah, *Langmuir* **28**, 4525 (2012).
- ⁴⁰M. Nishino, C. Enachescu, S. Miyashita, P. A. Rikvold, K. Boukheddaden, and F. Varret, *Sci. Rep.* **1**, 162 (2011).
- ⁴¹W. Nicolazzi, S. Pillet, and C. Lecomte, *Phys. Rev. B* **80**, 132102 (2009).
- ⁴²A. Slimani, K. Boukheddaden, F. Varret, H. Oubouchou, M. Nishino, and S. Miyashita, *Phys. Rev. B* **87**, 014111 (2013).
- ⁴³K. Boukheddaden, M. Nishino, and S. Miyashita, *Phys. Rev. B* **75**, 094112 (2007).
- ⁴⁴J. Jung, F. Bruchhäuser, R. Feile, H. Spiering, and P. Gütllich, *Z. Phys. B* **100**, 517 (1996).
- ⁴⁵N. D. Mermin, *Phys. Rev.* **176**, 250 (1968).
- ⁴⁶N. D. Mermin and H. Wagner, *Phys. Rev. Lett.* **17**, 1133 (1966).
- ⁴⁷P. Bruno, *Phys. Rev. Lett.* **87**, 137203 (2001).
- ⁴⁸S. V. Male'ev, *Sov. Phys. JETP* **43**, 1240 (1976).
- ⁴⁹M. Nishino, C. Enachescu, S. Miyashita, K. Boukheddaden, and F. Varret, *Phys. Rev. B* **82**, 020409 (2010).
- ⁵⁰C. Enachescu, M. Nishino, S. Miyashita, A. Hauser, A. Stancu, and L. Stoleriu, *Eur. Phys. Lett.* **91**, 27003 (2010).
- ⁵¹A. Slimani, F. Varret, K. Boukheddaden, C. Chong, H. Mishra, J. Haasnoot, and S. Pillet, *Phys. Rev. B* **84**, 094442 (2011).
- ⁵²J.-F. Létard, S. Asthana, H. J. Shepherd, P. Guionneau, A. E. Goeta, N. Suemura, Ryuta Ishikawa, and S. Kaizaki, *Chem. Eur. J.* **18**, 5924 (2012).
- ⁵³C. Chong, M. Itoi, K. Boukheddaden, E. Codjovi, A. Rotaru, F. Varret, F. A. Frye, D. R. Talham, I. Maurin, D. Chernyshov, and M. Castro, *Phys. Rev. B* **84**, 144102 (2011).
- ⁵⁴F. Condon, *Phys. Rev.* **32**, 858 (1928).
- ⁵⁵I. Maurin, private communication.
- ⁵⁶A. L. Edwards and H. G. Drickamer, *Phys. Rev.* **122**, 1149 (1961).
- ⁵⁷G. Rossi, R. Ferrando and C. Mottet, *Faraday Discuss.* **138**, 193 (2008).